Available online at www.sciencedirect.com
SCIENCE DIRECT®
Planetary and Space Science 52 (2004) 157–166
Planetary and Space Science
www.elsevier.com/locate/pss

SHARAD: The MRO 2005 shallow radar

R. Seu[a,*], D. Biccari[a], R. Orosei[b], L.V. Lorenzoni[c], R.J. Phillips[d], L. Marinangeli[e], G. Picardi[a], A. Masdea[a], E. Zampolini[f]

[a] *INFOCOM Department, University of Rome La Sapienza, Via Eudossiana, 18-00184 Rome, Italy*
[b] *CNR/IASF, Via del Fosso del Cavaliere, 100-00133 Rome, Italy*
[c] *ASI, Viale di Villa Grazioli, 23-00198 Rome, Italy*
[d] *Department of Earth and Planetary Sciences, Washington University, Campus Box 1169, One Brookings Drive, St. Louis, MO 63130, USA*
[e] *IRSPS-Universitá d'Annunzio, Viale Pindaro, 42-65127 Pescara, Italy*
[f] *Alenia Spazio, Via Saccomuro, 31-00131 Rome, Italy*

Received 2 April 2003; received in revised form 16 July 2003; accepted 29 August 2003

Abstract

SHARAD is a subsurface sounding radar provided by the Italian Space Agency (ASI) as a facility instrument to be flown on the NASA mission Mars Reconnaissance Orbiter (MRO). It shall be launched on August 2005 from the Cape Canaveral Air Force Station and shall deliver a payload designed to provide observations from a low Mars orbit with a nominal science period starting from October 2006. SHARAD operating parameters, 20 MHz central frequency with a 10 MHz bandwidth, shall allow to study the planet in a way that shall complement previous and recent results, shall be complementary to the other Italian sounding radar Mars Advanced Radar for Subsurface and Ionosphere Sounding (MARSIS) in terms of scale and resolution, and shall return scientific data for Martian soil in order to support the site selection for future landing missions. In this paper the scientific objectives and the system analysis will be discussed and the expected performance is evaluated.

Keywords: Mars; Subsurface; Radar sounding; Scattering models

1. Introduction

SHAllow RADar (SHARAD) is a subsurface sounding radar provided by ASI (Agenzia Spaziale Italiana, the Italian Space Agency) as a Facility Instrument to the NASA's 2005 Mars Reconnaissance Orbiter (MRO) mission for the characterisation of the upper Km of the Martian surface. MRO will be launched on August 2005 from the Cape Canaveral Air Force Station and will deliver a payload designed to provide observations from a low Mars orbit, with a nominal science period starting from October 2006. SHARAD operating parameters, a 20 MHz central frequency with a 10 MHz bandwidth, will allow to study the planet in a way that will be complementary to the Italian-US sounding radar Mars Advanced Radar for Subsurface and Ionosphere Sounding (MARSIS) (Picardi et al., 2003) in terms of scale and resolution, and will also be used to support the site selection for future landing missions.

The search for subsurface water has become a primary focus of Mars exploration. Its abundance and distribution (both as ground ice and groundwater) have important implications for understanding the geologic, hydrologic, and climatic evolution of the planet; the potential origin and continued survival of life and the accessibility of a critical in situ re-source for sustaining future human explorers. For these reasons, a principal goal of the Mars science, astrobiology, and the HEDS programs is to determine the 3-D distribution and state of subsurface H_2O, at a resolution sufficient to permit access to desired volatile targets by drilling. The three targets most often discussed are: groundwater, massive deposits of near-surface ground ice (e.g. associated with the ponded discharge of the outflow channels or the relic of a former ocean), and ice-saturated frozen ground. Based on the present best estimates of mean annual surface temperature, crustal thermal conductivity, geothermal heat flow, and groundwater freezing temperature, the mean thickness of frozen ground on Mars may vary from ~2.5–5 km at the equator to ~6.5–13 km at the poles (Clifford and Parker, 2001). However, natural variations in both crustal heat flow

* Corresponding author. Fax: +39-064873300.
E-mail address: robseu@infocom.ing.uniroma1.it (R. Seu).

0032-0633/$ - see front matter © 2003 Elsevier Ltd. All rights reserved.
doi:10.1016/j.pss.2003.08.024

and thermal conductivity are likely to result in significant local departures from these predicted values. For example, the lower thermal conductivities consistent with the surface thermal inertia imply that the base of the permafrost layer could be only hundreds of meters deep in places (Mellon and Phillips, 2001). The recent discovery of "young" fluvial-like features, emanating from the slopes of local scarps, raises the possibility that liquid water may also exist episodically at shallow ($\sim$ 100–500 m) depth (Malin and Edgett, 2000; Costard et al., 2002; Gilmore and Phillips, 2002); however, the true nature and absolute age of these features remains highly uncertain.

Reports by Boynton et al. (2002), Feldman et al. (2002) and Mitrofanov et al. (2002) present measurements from the newest NASA Mars orbital mission, Mars Odyssey, that appear to confirm the existence, predicted on theoretical grounds (e.g., Mellon and Jakosky, 1995), of large quantities of shallow subsurface ice (as inferred from hydrogen accumulations) in certain parts of the planet. Measurements of the neutron flux emitted from Mars in several different energy regimes and spectra of gamma-ray emissions induced by neutron capture reactions were used to map the global distribution of near-surface hydrogen on the planet. The abundance of hydrogen varies widely, the highest concentrations occurring pole-ward of about 60°N and 60°S, and is interpreted to indicate the presence of subsurface water (not CO_2) ice, on the basis of the specific patterns of neutrons detected and the spatial correlation to regions where ground ice has been predicted to be stable. Initial results indicate that the best fits for the enhanced hydrogen regions are consistent with a model surface with a "thin and dry" (few tens of centimetres; 1–2 wt% H_2O) upper layer overlying a "thick and ice-rich" (at least several hundred centimetres; 20–35 wt% H_2O) lower layer. Details on the thickness of the ice-rich lower layer are limited by the $\sim$ 1-m sensing depth of the neutron instruments, and it is not possible to determine the total quantity of subsurface ice present. However, if the modelling is correct, then the inferred ice concentration implies an extremely porous, nearly ice-filled regolith (the layer of rocky debris and dust resulting from repeated meteoritic impacts) at high latitudes. Separate lines of evidence suggest a loose and/or porous regolith that could exceed a kilometre or more in thickness, implying that the subsurface ice detected by Odyssey may represent only the tip of an iceberg frozen under ground (Bell, 2002).

2. Scientific objectives

The primary objective of the SHARAD experiment is to map, in selected locales, dielectric interfaces to several hundred meters depth in the Martian subsurface and to interpret these results in terms of the occurrence and distribution of expected materials, including competent rock, regolith, water and ice, with a vertical resolution of $\sim$ 10 m and a horizontal resolution of a few hundred meters (300 m–1 km). It is acknowledged that the surface of Mars will not be uniformly amenable to using radar sounding in the search for subsurface interfaces. However, it will be possible to find conditions of favourable radar viewing geometry, interface scattering, surface and volume scattering, and material properties, which may allow the identification of subsurface layers from orbit. When strong internal reflections do occur, they will be identifiable as aqueous only by contextual inferences drawn from the characteristic geological context of water habitats. Independent of any ability to directly detect water or ice, SHARAD should make significant new scientific data available toward addressing critical scientific problems on Mars, including the existence and distribution of buried paleo-channels, subsurface layering, an improved understanding of the electromagnetic properties of the "stealth" region, further insights into the nature of patterned ground, and other morphologies suggestive of the presence of water at present or in the past. In addition, it should be possible to answer certain kinds of geologic questions, such as the character of the surface below the polar ice caps and the nature of some of the layered terrains.

Although the belief that Mars is water-rich is supported by a wide variety of geologic evidence, current ignorance about the heterogeneous nature and thermal evolution of the planet's crust effectively precludes geomorphic or theoretical attempts to quantitatively assess in sufficient detail the current geographic and subsurface vertical distribution of ground ice and groundwater (Clifford, 1998). For this reason, any exploration activity (such as drilling) whose success is contingent on the presence of subsurface water, must be preceded by a comprehensive high-resolution geophysical survey capable of assessing whether local reservoirs of water and ice actually exist. Terrestrial experience has demonstrated that the accurate identification of such targets is likely to require the application of multiple geophysical techniques (Stoker, 1998).

Radar sounding from orbit, with the possibility of near-global coverage, offers a way out of the risks associated with landing a Ground Penetrating Radar (GPR) on the surface without prior knowledge of its site-specific subsurface structure. By sure GPR provides better spatial resolution in a limited area, however, there is simply no other way to obtain global data on the subsurface of Mars without using radar sounding—at least not at such cost-effectiveness. Moreover, the sun-synchronous orbit and the high data rate afforded by MRO provide an ideal situation for achieving a large coverage in favourable (i.e. night-time) conditions, with the extra bonus of overlapping passes offering an opportunity for 3-D mapping.

Probing the upper crust of Mars with radar in the 15–25 MHz frequency range is a unique way to study the planet, compared to all other investigations completed, in progress, or planned for the future. The only instrument comparable to SHARAD, which will be placed in orbit around Mars, is MARSIS (Mars Advanced Radar for Subsurface and Ionosphere Sounding, Picardi et al., 1998,

Table 1
Summary of the main system parameters of the MARSIS and SHARAD experiments

	MARSIS	SHARAD
Frequency bands	1.3–2.3 MHz, 2.5–3.5 MHz, 3.5–4.5 MHz, 4.5–5.5 MHz	15–25 MHz
Vertical resolution ($\varepsilon/\varepsilon_0 = 5$)	$\sim$ 70 m (1 MHz bandwidth)	$\sim$ 7 m (10 MHz bandwidth)
Penetration depth	$\sim$ 0.5 km to $\sim$ 5 km	$\sim$ 0.1 km to $\sim$ 1 km
Horizontal resolution (along-track $\times$ cross-track)	5–9 km $\times$ 15–30 km	0.3–1 km $\times$ 3–7 km

Table 2
Dielectric properties of reference categories of different Martian crust materials used to estimate the SHARAD performances

Category	ε'	$\tan\delta$
I-1	5	0.004
I-2	8	0.004
II-1	1.5	0.03
II-2	5	0.03
II-3	9	0.03
III	7.1	0.014

The categories cover a wide range of magmatic rocks (basaltic to andesitic in composition), low-grade metamorphic rocks and sedimentary rocks (claystones, sandstones, limestones).

1999, 2003), on board ESA's Mars Express spacecraft. Operating in the 1–5 MHz frequency range, the penetration depths expected for MARSIS, up to 5 km, will open up a new realm in the study of Martian crustal properties and geologic processes, detection of subsurface ice and liquid water being the main goal of the experiment. MARSIS, however, has a relatively coarse resolution, and was conceived to test hypotheses on global models of subsurface water and ice distribution. New results on the distribution of subsurface water on Mars, brought by Mars Global Surveyor (MGS) and Mars Odyssey, have prompted the need for an instrument complementing the results of MARSIS. An instrument able to penetrate a few hundreds of meters below the surface with a finer horizontal resolution and with a vertical resolution on the order of 10–20 m would provide a unique insight into Martian stratigraphy. This would offer a potentially significant improvement in the understanding of sedimentary processes and geologic activity. The main system parameters of the two sounders are summarised in Table 1.

3. System analysis

The ability of SHARAD to achieve its science objectives will be largely dependent on the electrical properties, both permittivity and permeability, of the soil, degree of scattering off the surface and volumetric debris, and the stratigraphical layering of the subsurface.

The available data allow a broad characterization of the Martian surface composition (Bandfield et al., 2000), that is a basaltic composition in the southern hemisphere, and an andesitic composition in the north. Although a multitude of different materials is likely present at the surface of Mars, it is necessary, to the purpose of an engineering system analysis, to select a few representative dielectric constants as most meaningful for electromagnetic modeling (Picardi et al., 1998). Table 2 shows a reference summary of the representative categories of possible materials detailing the real part of their dielectric constant and their loss tangent.

Two simple layering models have been used for a first preliminary analysis of the theoretical detection capabilities of subsurface water and ice. In the first of these two models, called (I/W), the first layer is a porous crust with the pores filled up by ice from the surface down to a depth below which liquid water is stable and becomes the pore-filling material. In the second model, called (D/I), the pore-filling material of the first layer is considered to be a gas or some other vacuum-equivalent material down to a depth, below which ice fills the pores.

The dielectric properties of the mixtures of the different materials in the above mentioned models, have been evaluated as in Picardi et al. (1998) according to the well known Maxwell–Garnett model. It is worth noting that for this evaluation a model for the variation of the Martian crust porosity as a function of depth also has been considered (Clifford, 1993; Binder and Lange, 1980): according to that model the porosity should follow the exponential law

$$\Phi(z) = \Phi(0)\exp(-z/K), \tag{1}$$

where $\Phi(0)$ is the porosity at the surface and K is a gravitationally-scaled decay constant ($\approx$ 2.82 km for Mars, Clifford, 1993). The globally-averaged porosity at the surface of Mars is expected to be in the range of 0.2–0.5 (Clifford, 1993).

Considering now the surface scattering characteristics, an attempt has been made to assess the extent and distribution of the surface clutter (i.e. the echoes from off-nadir portions of the surface which can mask the time synchronous echoes reflected from the wanted subsurface layers) making also use of the Mars Orbiter Laser Altimeter (MOLA) data. To this purpose it has been assumed that the topography is self-affine, i.e. statistical parameters change with scale according to a power law: the exponent of such law is called the Hurst exponent H (Orosei et al., 2003).

Topography is usually modelled as an instance of a random process, and, as such, it is characterised by means of statistical parameters. Most commonly, assumptions are made on the distribution of quantities such as topographic heights and slopes, and real topographic data are used to compute the parameters of those distributions.

The simplest models describe the topographic height as a Gaussian-distributed stationary random variable. The most important moment of the distribution is the standard deviation, which is estimated by computing the root-mean-squared (rms) height of discrete samples of the topography along profiles or grids.

Another property of topography is slope, i.e. the difference in height between two points divided by their distance, and its statistical distribution. Slope has also been modelled as a stationary random variable, and it is usually characterised by means of its standard deviation. In a discretely sampled topographic profile, this quantity can be estimated by means of the rms slope s, which is defined as the rms difference in height between points divided by their lag or step.

These parameters are routinely computed for the statistical analysis of topography, both on Earth and in other planetary bodies (e.g., for Mars, Aharonson et al., 1998, 2001; Garvin and Frawley, 2000; Garvin et al., 1999; Kreslavsky and Head, 1999, 2000; Smith et al., 1999, 2001), and to model electromagnetic scattering from natural surfaces (e.g. Ulaby et al., 1986; Ogilvy, 1991), typically making use of hypotheses on the shape of the autocorrelation function of the surface.

This description of topography, however, does not account for a commonly observed property, that of scale dependence: rms slope depends on the horizontal distance between points Δx, and rms height changes in topographic profiles of the same area with different lengths. It is found that this behaviour can be described by power laws:

$$s(\Delta x) = s_0 \left(\frac{\Delta x}{\Delta x_0} \right)^{H-1},$$

where s_0 is the RMS slope of the profile computed at distance Δx_0 between points and H is the Hurst exponent ($0 < H < 1$). These observations have led to the modelling of topography as a non-stationary random variable by means of self-affine fractals. Self-affinity is the scaling behaviour of a topographic surface such that increasing the scale of the x and y axes by a factor r must be compensated for in the z direction by a factor r^H for the surface to remain statistically identical.

Moreover the Mars Orbiter Camera (MOC) images have revealed the existence of boulder fields on the Martian surface; however, a survey of 25,000 high-resolution MOC images (Golombek, 2001) revealed that only $\sim 0.1\%$ of the total shows fields of hundred to thousands of boulders. For this reason we have considered the contribution of these boulders to the surface scattering to be negligible.

Volumetric scattering has been estimated as in Picardi et al. (1998), obtaining a worst-case cross-section per unit volume of about 3.7×10^{-2}. On average, however, the cross-section per unit volume should be 8.6×10^{-4}.

Table 3
Surface Fresnel reflectivity

Scenario $\Phi(0)$	$\Gamma_s\|_{\mathrm{dB}}$			
	I/W		D/I	
	50%	20%	50%	20%
I-1	−9.5	−9	−12	−9.5
I-2	−8	−7	−9.5	−7.5
II-1	−14	−17	−25.5	−22
II-2	−9.5	−9	−12.5	−9.5
II-3	−7.5	−6.5	−9	−7
III	−8.5	−7.5	−10	−8

Subsurface signals must compete with clutter signals arising from surface reflectors at the same radar delay. Assuming as a first approximation that the surface and subsurface interfaces have the same average topographic characteristics, the ratio of the above mentioned surface and subsurface echoes is directly proportional to the corresponding Fresnel reflectivities. The Fresnel reflectivity (for nadir incidence) of the Martian crust for the different material categories reported above is provided in Table 3.

The Fresnel reflectivity of a subsurface layer located at a depth z is given by

$$\Gamma_{\mathrm{SS},z} = R_{12,z}^2 (1 - R_{01}^2)^2 \times 10^{-0.1 \int_0^z \alpha(\zeta)\,\mathrm{d}\zeta} \tag{2}$$

being $R_{12,z}^2$ the Fresnel reflectivity of the subsurface interface, R_{01}^2 the Fresnel reflectivity of the surface, and $\alpha(\zeta)$ the two-way attenuation in dB per meter due to the dielectric dissipation in the crust, given by

$$\alpha_{\mathrm{dB}}(\varsigma) = 1.8 \times 10^{-7} f_0 \sqrt{\varepsilon} \tan \delta. \tag{3}$$

An evaluation of the Fresnel reflectivity for different subsurface layers, once again for the different categories of materials considered above, which results almost independent of either the depth z (in the first km of the crust), and of the attenuation are reported in Table 4.

The Martian surface back-scattering coefficient can be evaluated by introducing a fractal geometric description of the surface in the classical Kirchhoff approximation of the scattered electric field from a random rough surface. With this hypothesis, the backscattering coefficient can be written as (Picardi et al., 2001):

$$\sigma_0(\theta) = \frac{|R(0)|^2}{H \cos^2 \theta} \left[\frac{(2\pi)^{(H-1)/H}}{[s(\lambda)]^{1/H} \sqrt{2}^{1/H} (\cos\theta)^{1/H}} \right]^2 \times \sum_{s=0}^{\infty} (-1)^s \frac{\sin^{2s} \vartheta}{(s!)^2} \left[\frac{(2\pi)^{(H-1)/H}}{[s(\lambda)]^{1/H} \sqrt{2}^{1/H} (\cos\theta)^{1/H}} \right]^{2s} \times \Gamma\left(\frac{s+1}{H} \right), \tag{4}$$

Table 4
Reflection coefficient of the subsurface interfaces and attenuation of the first layer per km and per MHz

Scenario $\Phi(0)$	$R_{12}\|_{dB}$				$\alpha_{dB/km\ MHz}$			
	I/W		D/I		I/W		D/I	
	50%	20%	50%	20%	50%	20%	50%	20%
I-1	−10	−17.5	−21	−29.5	0.95	1.3	1	1.3
I-2	−9.5	−17	−23	−32	1.2	1.7	1.3	1.7
II-1	−13.5	−21	−17	−25	4.4	5.8	3.8	5.5
II-2	−10	−17.5	−21	−29	7	10	7.5	10
II-3	−9.5	−17	−24	−33	9.5	13.5	10.5	14
III	−9.5	−17	−22.5	−31.5	3.9	5.5	4.3	5.5

where $|R(0)|^2$ is the Fresnel reflection coefficient, $s(\lambda)$ is the wavelength-scale rms slope of the surface and $\Gamma(x)$ is the Gamma function. Eq. (4) gives, for $H = 1$, the well-known geometric optics model (Simpson and Tyler, 1982) and, for $H = 0.5$, the Hagfors model (Hagfors, 1964). The behavior of the surface clutter as a function of the off-nadir angle θ can be easily computed in these two cases of the geometric optics and Hagfors models, which represent end-members for the majority of the Martian surface geometry (see Table 1): the corresponding evaluation will be discussed in the following section.

Finally, by considering the requirement on the penetration depth and a possible dynamic range of the useful signals of about 50 dB, evaluated for a reasonable set of crust materials (see the Tables 2 and 4), a transmitted frequency of 20 MHz seems to be attainable, thus reducing the ionosphere propagation and Faraday rotation problems encountered at lower frequencies. The required bandwidth should be on the order of 10 MHz in order to obtain a free-space range (depth) resolution of 15 m. The required ground resolution is obtained via the classical pulse-limited geometry in the cross track direction and via synthetic aperture processing in the along-track direction. Collection of sufficient coherent data takes up to about a couple of seconds to achieve the better resolution required, that is 300 m. It is worth noting that the requirements on the Spacecraft motion and attitude needed to perform this synthetic aperture processing are well within the capabilities of the mission ephemeris reconstruction, mainly driven by the high resolution imaging instruments on board the MRO, so that this kind of processing does not impose particular constraints.

4. Performance evaluation

A preliminary sizing of the radar sounder requires the evaluation of the link budget with sounding assumptions for its relevant parameters which will guide the design of the SHARAD instrument.

The single-look signal-to-noise ratio for non-coherent surface back-scattering is given by (Picardi et al., 1999, 2003):

$$\frac{S}{N} = \frac{P_p G^2 \lambda^2 \sigma^0 A}{(4\pi)^3 R^4 K T_S L} \tau N = \frac{P_p G^2 \lambda^3 \sigma^0}{(4\pi)^3 R^3 K T_S L} \sqrt{2R\Delta}\, \frac{DC.}{V_t}$$
$$= \frac{P_p G^2 \lambda^3 \sigma^0 \sqrt{2\Delta} DC}{(4\pi)^3 R^{2.5} K T_S L V_t}, \quad (5)$$

where P_p is the peak power, G the antenna gain, λ the wavelength, σ^0 the surface backscattering coefficient, A the area of the ground resolution cell, τ the transmitted pulse width, N the number of coherently integrated pulses within the synthetic aperture, R the range, K the Boltzmann constant, T_S the system temperature, L the propagation losses and $A\tau N = R_{AZ} 2\sqrt{2R\Delta}\tau(L_S/V_t)PRF = (\lambda R/V_t)\sqrt{2R\Delta}DC$, being R_{AZ} the along track resolution, Δ the range resolution, L_S the length of the synthetic aperture, PRF the pulse repetition frequency, V_t the spacecraft tangential velocity and $DC = \tau\, PRF$ the system duty cycle.

To evaluate the radar equation in Eq. (5) it is assumed that the peak power radiated by the antenna is 10 W (which is a specification requirement to the design of the transmitter), the range resolution in free space is 15 m, the average altitude is 300 km and the duty cycle is about 5%. Regarding the *PRF* it is worth to note that its value cannot be established uniquely from the need to avoid overlap between transmitted pulses and received echoes. Synthetic aperture processing requires additionally that aliasing in the observed Doppler spectrum must be avoided. Provided that SHARAD will use a dipole antenna and considering the clutter formulation of Eq. (4), the final value of the *PRF* (about 700 Hz) has been selected in order to ensure a limited impact of the aliasing.

The link budget with the above mentioned system assumptions is shown in Table 5, where σ^0 is evaluated by means of Eq. (4): the surface reflectivity is between −7 and −17 dB for the I/W scenario, and between −7 and −25 dB for the D/I scenario; the rms slope $s(\lambda)$ is between 0.006 and 0.1.

The surface return echoes can be considered as surface clutter, because the subsurface discontinuity detection could be reduced by the surface backscattering. Then the backscattering coefficient, as in Eq. (4), can be related to the

Table 5
Surface signal-to-noise ratio after coherent integration

Scenario	I/W S/N dB	D/I S/N dB
P_p (10 W)	10	10
G^2	0	0
λ^3	35	35
σ^0	54–0	54 to −8
$64\pi^3$	−33	−33
$R^{2.5}$ ($R = 300$ km)	−137	−137
$K(=1.38 \times 10^{-23})$	228	228
$T_S L$ (Braun Model)	−49	−49
$\sqrt{2\Delta}$ ($\Delta = 15$ m)	7	7
DC (5%)	−13	−13
V_0 (4 km/s)	−36	−36
Single look S/N	66–12	66–4

penetration depth δ in terms of equivalent off-nadir angle of the incoming interfering clutter:

$$\theta = \sqrt{\frac{2\delta\sqrt{\varepsilon}}{R}}. \tag{6}$$

If the surface and subsurface interfaces have the same roughness, the signal-to-clutter ratio is given by

$$\left.\frac{S}{C}\right|_{\mathrm{dB}} \cong R_{12}|_{\mathrm{dB}} - \alpha_{\mathrm{dB/m}}\delta - \Gamma_s|_{\mathrm{dB}} - 10\log\left(\exp\left(-\frac{2\sqrt{\varepsilon}\delta}{2Rs^2(\lambda)}\right)\right) \tag{7}$$

for $H = 1$ (Simpson and Tyler, 1982), and

$$\left.\frac{S}{C}\right|_{\mathrm{dB}} \cong R_{12}|_{\mathrm{dB}} - \alpha_{\mathrm{dB/m}}\delta - \Gamma_s|_{\mathrm{dB}} + 15\log\left(1 + \frac{2\sqrt{\varepsilon}\delta}{4\pi^2 s^4(\lambda)R}\right) \tag{8}$$

for $H = 0.5$ (Hagfors, 1964). Table 6 shows the parameters of Eqs. (7) and (8) for the selected reference models.

It is worth noting that, according to Eq. (6), the last term of Eqs. (7) and (8) represent the decrease of the surface clutter with the off-nadir angle, and can be considered as an improvement factor (IF) of the signal-to-clutter ratio when both the signal and the clutter are evaluated at nadir incidence. Taking into account the values of the IF reported in Table 6c, evaluated for different surface slopes and penetration depths and, just as an example, for $\varepsilon = 5$, it is possible to arrive at the conclusion that this IF is negligible in the worst case of very rough surfaces, no matter what the Hurst exponent is. Taking also into account the increase of the IF that can be achieved by means of the Doppler processing, as discussed below, we can estimate the maximum depth at which the subsurface echo is still observable as the depth at which the signal to clutter ratio is equal to −30 dB. The results are shown in Table 7.

Table 6
Values of the terms (a) due to the Fresnel reflectivity of the surface and subsurface interfaces. (b) Due to dielectric losses. (c) Geometric contribution to the signal-to-clutter ratio

(a) *Values of the terms due to the Fresnel reflectivity*

Scenario $\Phi(0)$	$R_{12\|\mathrm{dB}}$-$\Gamma_{s\|\mathrm{dB}}$			
	I/W		D/I	
	50%	20%	50%	20%
I-1	−0.5	−8.5	−8.5	−20
I-2	−1.5	−10	−13.5	−25
II-1	0.5	−4	8	−3.5
II-2	−0.5	−9	−8.5	−20
II-3	−2	−10	−15	−26
III	−1	−10	−12	−23

(b) *Values of the terms due to dielectric losses*

Scenario $\Phi(0)$	$\alpha_{\mathrm{dB/(100\ m)}}$ (20 MHz)			
	I/W		D/I	
	50%	20%	50%	20%
I-1	2	2.5	2	2.5
I-2	2.5	3.5	2.5	3.5
II-1	8	11.5	7.5	11
II-2	12	20	14	20
II-3	17	27	20	28
III	8	11	8	11

(c) *Geometric contribution to the signal-to-clutter ratio*

s_λ		$-10\log\left(\exp\left(-\frac{2\sqrt{\varepsilon}\delta}{2Rs_\lambda^2}\right)\right)$ Geometric optics	$15\log\left(1+\frac{2\sqrt{\varepsilon}\delta}{4\pi^2 s_\lambda^4 R}\right)$ Hagfors model
0.1	200	0.65	3.6
	300	1	5
0.05	200	2.6	16.7
	300	3.9	19.2
0.01	200	64	58
	300	97	61

5. Hardware description

Key elements for the radar design are represented by the identified center frequency, 20 MHz, the bandwidth of the radar pulse equal to 10 MHz, and the requested spatial resolution that should range between 300 and 1000 m.

Similarly to the MARSIS radar, SHARAD can be then conceived around 3 major subsystems: Antenna S/S, RF S/S, and Digital S/S. The antenna will be essentially composed of a dipole radiating element roughly matched in length to half the wavelength of the carrier frequency. An

Table 7
Maximum sounding depth compatible with a signal-to-clutter ratio of −30 dB

Scenario $\Phi(0)$	Max. penetration depth (km)			
	I/W		D/I	
	50%	20%	50%	20%
I-1	1.5	0.7	1	0.3
I-2	1.5	0.7	1	0.3
II-1	0.4	0.35	0.4	0.3
II-2	0.25	0.2	0.1	0.05
II-3	0.15	0.1	—	—
III	0.4	0.3	0.15	0.1

impedance matching network will also be required to match the transmitter and antenna impedances. The RF S/S, envelops the Transmitter, the Tx/Rx switching net and the receiver down to the Analog to Digital Converter. The Digital S/S envelopes the Command and Control functions interfacing with the spacecraft bus, the processing capabilities to pre-elaborate the science data collected during the observations, as well as the digital synthesis of the radar pulse and generation of the system timings.

The radar shall be able to transmit frequency modulated radar pulses of about 85 μs length and bandwidth of 10 MHz. To cope with the 300–1000 m spatial resolution requirement, SHARAD shall actually operate as a nadir looking synthetic aperture radar sounder. Synthetic aperture processing also referred as Doppler filtering, aids reduction of off-nadir, along-track clutter disturbance, improving the sub-surface detectability by roughly 10 dB. On the opposite it can be easily demonstrated that, for the indicated resolution figures, a fully focused synthetic aperture processing is required.

Moreover in order to improve the subsurface detectability, the same synthetic aperture concept could also be applied in the cross-track direction by processing, on ground on a best effort basis, the coherent data taken from many appropriate close orbits if available. Different non-coherent processing techniques are under analysis as well.

The SHARAD proposed concept is aimed to a HW design which meets the mission constraints. Current best estimates indicate roughly 17 kg for the mass and 44 W for the peak power during science observations.

6. Science data

The Martian ionosphere poses a major limitation on low-frequency wide-bandwidth radar observations of the surface and subsurface. At these frequencies, frequency-dependent propagation delays (dispersion) will degrade the signal, and different frequencies will suffer different delays, an effect whose severity increases with relative bandwidth and with proximity of the radar's band to the maximum plasma frequency. Through the Chapman theory of planetary ionospheres, it is estimated that the lowest frequency that can penetrate the Martian ionosphere varies from about 4 MHz on the day side of Mars to somewhat below 1 MHz on the night side. Having a much higher frequency range, however, SHARAD is in principle able to operate at any time in the orbit, independently of the Sun illumination conditions.

During its normal operation SHARAD will be an open-loop controlled instrument switching among different modes of operation according to a pre-determined sequence of commands. Within a single orbit, the instrument can be operated in any of its observation modes, in any desired sequence, either continuously or discontinuously. The time limit is set by the portion of overall data volume allocated to SHARAD vs. the selected operational modes, while the choice of the orbits in which the instrument will operate is largely set by a non-interference rule with down-link to the DSN.

SHARAD is a surveying instrument, in which meaningful observations are built by multiple data collections over a given area of interest. Because of this, and because MARSIS will provide data on subsurface structure with a limited spatial resolution, the vast majority of SHARAD observations will be planned in terms of passages over target regions that will extend several tens or hundreds of kilometers, rather than in terms of point-like data acquisitions as in optical imaging instruments.

It is currently expected that MRO will downlink a geometrical mean of at least 7.2 Gb of SHARAD data per day, although this quantity will vary considerably according to constraints and opportunities arising from operations planning. The data volume allocated to SHARAD over the entire MRO mission is currently set at 15% of the total: this corresponds to 4 Tb of raw data being produced by the instrument during approximately one Martian year. Dividing this number by the instrument data rate, it is estimated that the total time of data taking will be sufficient to achieve global coverage with a minimum spacing of 10 km at the equator, if observation opportunities are provided over the entire surface of the planet.

Chirp radars, like SHARAD, are used when the length of the pulse for the desired range resolution is so short that to achieve good signal-to-noise ratio the pulse would require a peak power exceeding the limits imposed by the mission design. The chirp, a longer pulse that is modulated in frequency (for SHARAD, the modulation is a linear frequency sweep, as in MARSIS), allows a resolution that depends on the bandwidth: with a bandwidth B, the approximate time resolution of the output pulse after processing is $1/B$, and if the transmitted amplitude is constant during the pulse, the output takes the form of a $\sin x/x$ pulse whose amplitude is $B\tau$ times the amplitude of the input signal (Cook and Bernfeld, 1967), where τ is the chirp duration. This process, called range compression, is performed on ground for SHARAD, on the digitally sampled data, to properly compensate

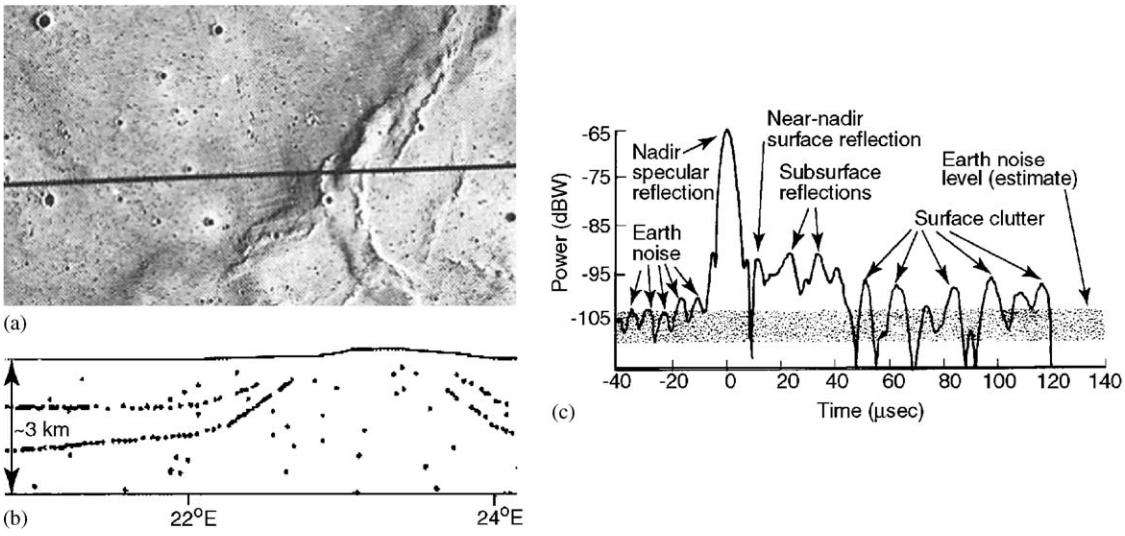

Fig. 1. An example of data from the Apollo Lunar Sounder Experiment (ALSE) on-board Apollo 17, the only orbiting subsurface-sounding radar for which data currently exist (modified from Peeples et al., 1978). (a) A segment of the Apollo 17 ground track for revolution 16 in Mare Serenitatis. (b) Coherent ALSE radar returns, with surface clutter largely removed, drawn to the same horizontal scale. (c) A power versus time trace of the digital data from a single radar echo. Time is arbitrarily referenced to zero at the nadir specular reflection.

ionospheric effects: accurate coherent pulse compression requires in fact detailed knowledge of the modulation of the returning signals, whose phase structure is distorted in their (two-way) propagation through the ionosphere.

SHARAD on-board processing of the pulse echoes consists in artificially adding a delay, corresponding to a phase shift, to the samples of each pulse, and then in summing the samples so as to allow the constructive sum of the signal component whose delay (phase shift) from one pulse to the next corresponds to the nadir direction. This is called synthetic aperture processing, and is used to improve both horizontal resolution in the along-track direction and signal-to-noise ratio: horizontal resolution becomes that of an equivalent antenna whose length is equal to the segment of the spacecraft trajectory over which pulse echoes are summed coherently, whereas signal-to-noise ratio improves by a factor equal to the number of coherently summed pulses (see Eq. (5)).

SHARAD performs unfocussed on-board processing on the samples, which reduces data rate by a factor of up to 32: the use of more sophisticated processing schemes, further reducing data rate, is limited by the accuracy of the spacecraft ephemeris required to correctly perform the coherent sum of signal samples. Further synthetic aperture processing of SHARAD pre-summed echoes will take place on the ground and is conceptually identical to on-board processing, except that phase correction accounts for the curvature of the sampled wave-front, using reconstructed orbit data: this allows for the longer synthetic apertures which are needed to achieve the desired along-track horizontal resolution, which will range between 300 and 1000 m.

Calibrated echo profiles will be produced following standard procedures for radar signal processing and building on MARSIS experience. The data products will be relatively model independent, although the optimum choice of the processing parameters will require some subjectivity. An example of a radar echo after aperture synthesis and range compression is shown in Fig. 1(c). It can be seen that several features not due to subsurface reflection are still present in the signal, caused by off-nadir surface reflections (surface clutter). Radargrams, i.e. 2-D (ground distance, time delay) images in which the dependent variable is calibrated power, can be produced by collating and stacking individual echoes along track: an example is provided in Fig. 1(b), in which continuous subsurface layers can be clearly discerned. In this figure, clutter was largely removed by applying stereo methods on adjacent, parallel orbits.

Thus, sections of the dielectric properties of the shallow crust will be produced, which, as coverage accumulates, will constitute a full three-dimensional description of the Martian subsurface structure. These data will provide a unique ability to map the subsurface distribution of water on a global basis with a single spacecraft. Such a reconnaissance would likely also yield significant new insights regarding the subsurface structure and lithology of the crust, including the nature of the polar layered deposits. Although the unambiguous identification of a specific volatile target is probably not possible using orbital sounding alone, it provides the only approach for achieving global coverage of this important data type.

Beyond individual radar echoes and radargrams, maps of surface reflectivity, elevation and roughness will be produced, through higher-level processing of radar pulses. Maps will be created as coverage accumulates, and it is possible that early releases can be generated, being updated during the course of the mission.

7. Conclusions

In this paper, the design of a shallow, high resolution subsurface radar for the search of subsurface water on Mars has been illustrated. This radar, named SHARAD, will be flown on NASA's Mars Reconnaissance Orbiter in 2005.

In the radar design process, models of the Martian stratigraphy have been considered, based on the dielectric characteristics of materials that are deemed to constitute the Martian crust. Then, the backscattering characteristics of the Martian topography have been analyzed, in order to understand how undesired surface echoes (clutter) limit the detection of subsurface features. Finally, an optimization of the radar system parameters, namely carrier frequency, bandwidth, dynamic range and sensitivity, has been carried out to define the main requirements of the radar: SHARAD is designed to detect subsurface interfaces down to about 1 km depth, due to the low carrier frequency of 20 MHz; to have a vertical resolution in the order of 15 m, due to the transmitted bandwidth of 10 MHz; to achieve a sidelobe control of 50 dB for the expected dynamic range; and to obtain a ground resolution in the order of a few hundred meters to a few km. It has been found that, even without dedicated processing devoted to surface clutter cancellation, a large part of the Martian surface, including the poles, can be analyzed with the SHARAD experiment.

SHARAD continues the probing started with MARSIS to "follow the water" by directly detecting ice and possible aquifers, with an increased likelihood of success due to the mission design. The capability to probe the upper 1 km at high resolution allows testing of hypotheses of recent shallow water reservoirs, and feeds forward to characterization and selection of possible sites for drilling experiments in 2007 and beyond. While SHARAD will benefit from MARSIS design heritage, the design of a 2005 sounder cannot benefit from MARSIS data due to the close consecutive launch opportunities. Consequently, most risks associated with uncertainties in the Mars environment (ionosphere, attenuation in the crust, nature of interfaces) will apply to both MARSIS and SHARAD.

References

Aharonson, O., Zuber, M.T., Neumann, G.A., Head, J.W., 1998. Mars: Northern hemisphere slopes and slope distributions. Geophys. Res. Lett. 25, 4413–4416.

Aharonson, O., Zuber, M.T., Rothman, D.H., 2001. Statistics of Mars' topography from the Mars Orbiter Laser Altimeter: slopes, correlations, and physical models. J. Geophys. Res. 106, 23723–23735.

Bandfield, J.L., Hamilton, V.E., Christensen, P.R., 2000. A global view of Martian surface compositions from MGS-TES. Science 286, 1626–1630.

Bell III, J.F., 2002. Tip of the Martian iceberg? Science 297, 60–61.

Binder, A.B., Lange, M.A., 1980. On the thermal history, thermal state, and related tectonism of a Moon of fission origin. J. Geophys. Res. 85, 3194–3208.

Boynton, W.V., Feldman, W.C., Squyres, S.W., Prettyman, T.H., Brückner, J., Evans, L.G., Reedy, R.C., Starr, R., Arnold, J.R., Drake, D.M., Englert, P.A.J., Metzger, A.E., Mitrofanov, I., Trombka, J.I., d'Uston, C., Wänke, H., Gasnault, O., Hamara, D.K., Janes, D.M., Marcialis, R.L., Maurice, S., Mikheeva, I., Taylor, G.J., Tokar, R., Shinohara, C., 2002. Distribution of hydrogen in the near surface of Mars: evidence for subsurface ice deposits. Science 297, 81–85.

Clifford, S.M., 1993. A model for the hydrologic and climatic behaviour of water on Mars. J. Geophys. Res. 98, 10973–11016.

Clifford, S.M., 1998. Mars: the effect of stratigraphic variations in regolith diffusive properties on the evolution and vertical distribution of equatorial ground ice. 29th Annual Lunar and Planetary Science Conference, Lunar and Planetary Institute, Houston, TX, abstract no. 1922.

Clifford, S.M., Parker, T.J., 2001. The evolution of the Martian hydrosphere: implications for the fate of a primordial ocean and the current state of the northern plains. Icarus 154, 40–79.

Cook, C.E., Bernfeld, M., 1967. Radar Signals. Academic Press, New York, London.

Costard, F., Forget, F., Mangold, N., Peulvast, J.P., 2002. Formation of recent Martian debris flows by melting of near-surface ground ice at high obliquity. Science 295, 110–113.

Feldman, W.C., Boynton, W.V., Tokar, R.L., Prettyman, T.H., Gasnault, O., Squyres, S.W., Elphic, R.C., Lawrence, D.J., Lawson, S.L., Maurice, S., McKinney, G.W., Moore, K.R., Reedy, R.C., 2002. Global distribution of neutrons from Mars: results from Mars Odyssey. Science 297, 75–78.

Garvin, J.B., Frawley, J.J., 2000. Global vertical roughness of Mars from Mars Orbiter Laser Altimeter pulse-width measurements. 31st Annual Lunar and Planetary Science Conference, Lunar and Planetary Institute, Houston, TX, abstract no. 1884.

Garvin, J.B., Frawley, J.J., Abshire, J.B., 1999. Vertical roughness of Mars from the Mars Orbiter Laser Altimeter. Geophys. Res. Lett. 26, 381–384.

Gilmore, M.S., Phillips, E.L., 2002. Role of aquicludes in formation of Martian gullies. Geology 30, 1107–1110.

Golombek, M.P., 2001. Extreme rock distributions on Mars. 32nd Annual Lunar and Planetary Science Conference, Lunar and Planetary Institute, Houston, TX, abstract no.1116.

Hagfors, T., 1964. Backscattering from an undulating surface with applications to radar returns from the Moon. J. Geophys. Res. 69, 3779–3784.

Kreslavsky, M.A., Head, J.W., 1999. Kilometer-scale slopes on Mars and their correlation with geologic units: initial results from Mars Orbiter Laser Altimeter (MOLA) data. J. Geophys. Res. 104, 21911–21924.

Kreslavsky, M.A., Head, J.W., 2000. Kilometer-scale roughness of Mars: results from MOLA data analysis. J. Geophys. Res. 105, 26695–26711.

Malin, M., Edgett, K., 2000. Evidence for recent groundwater seepage and surface runoff on Mars. Science 288, 2330–2335.

Mellon, M.T., Jakosky, B.M., 1995. The distribution and behaviour of Martian ground ice during past and present epochs. J. Geophys. Res. 100, 11781–11799.

Mellon, M.T., Phillips, R.J., 2001. Recent gullies on Mars and the source of liquid water. J. Geophys. Res. 106, 23165–23179.

Mitrofanov, I., Anfimov, D., Kozyrev, A., Litvak, M., Sanin, A., Tret'yakov, V., Krylov, A., Shvetsov, V., Boynton, W.V., Shinohara, C., Hamara, D., Saunders, R.S., 2002. Maps of subsurface hydrogen from the High Energy Neutron Detector, Mars Odyssey. Science 297, 78–81.

Ogilvy, J.A., 1991. Theory of Wave Scattering From Random Rough Surfaces. Institute of Physics Publishing, Bristol, Philadelphia.

Orosei, R., Bianchi, R., Coradini, A., Espinasse, S., Federico, C., Ferriccioni, A., Gavrishin A.I., 2003. Self-affine behavior of Martian topography at kilometer scale from Mars Orbital Laser Altimeter data. J. Geophys. Res. 28 10.1029/2002JE001883.

Peeples, W.J., Sill, W.R., May, T.W., Ward, S.H., Phillips, R.J., Jordan, R.L., Abbott, E.A., Killpack, T.J., 1978. Orbital radar evidence for lunar subsurface layering in Maria Serenitatis and Crisium. J. Geophys. Res. 83, 3459–3468.

Picardi, G., Plaut, J.J., Johnson, W.T.K., Borgarelli, L., Jordan, R.L., Gurnett, D., Sorge, S., Seu, R., Orosei, R., 1998. The subsurface sounding radar altimeter in the Mars Express mission, proposal to ESA, INFOCOM Document n. N188-23/2/1998.

Picardi, G., Sorge, S., Seu, R., Fedele, G., Federico, C., Orosei, R., 1999. Mars Advanced Radar for Subsurface and Ionosphere Sounding (MARSIS): models and system analysis. INFOCOM Technical Report 007/005/99.

Picardi, G., Biccari, D., Seu, R., Orosei, R., 2001. Mars fractal topography applied to Radar for Subsurface and Ionosphere Sounding (MARSIS). XXVI General Assembly of the European Geophysical Society, Nice, France. Geophys. Res. Abstr. 3, CD-ROM edition.

Picardi, G., Biccari, D., Seu, R., Plaut, J.J., Johnson, W.T.K., Jordan, R.L., Gurnett, D.A., Orosei, R., Bombaci, O., Provvedi, F., Zampolini, E., 2003. Mars Advanced Radar for Subsurface and Ionosphere Sounding (MARSIS). Planet. Space Sci., doi:10.1016/j.pss.2003.08.020.

Simpson, R.A., Tyler, G.L., 1982. Radar scattering laws for the lunar surface. IEEE Trans. Antennas Propagat. AP-30, 438–449.

Smith, D.E., et al., 1999. The global topography of Mars and implications for surface evolution. Science 284, 1495–1503.

Smith, D.E., et al., 2001. Mars Orbiter Laser Altimeter (MOLA): experiment summary after the first year of global mapping of Mars. J. Geophys. Res. 106, 23689–23722.

Stoker, C., 1998. Mars Deep Water Sounding Workshop Summary, http://astro-biology.arc.nasa.gov/worshops/1998/marswater/index.html.

Ulaby, F.T., Moore, R.K., Fung, A.K., 1986. Microwave Remote Sensing: Radar Remote Sensing and Surface Scattering and Emission Theory, Vol. 2. Artech House, Norwood, 1986.